

Superdiffusive dispersals impart the geometry of underlying random walks

V. Zaburdaev,^{1,2} I. Fouxon,³ S. Denisov,^{4,5,6} and E. Barkai³

¹Max Planck Institute for the Physics of Complex Systems,
Nöthnitzer Strasse 38, D-01187 Dresden, Germany

²Institute of Supercomputing Technologies, Lobachevsky State University of Nizhny Novgorod, 603140 N. Novgorod, Russia

³Department of Physics, Institute of Nanotechnology and Advanced Materials, Bar-Ilan University, Ramat-Gan, 52900, Israel

⁴Department of Applied Mathematics, Lobachevsky State University of Nizhny Novgorod, 603140 N. Novgorod, Russia

⁵Sumy State University, Rimsky-Korsakov Street 2, 40007 Sumy, Ukraine

⁶Institute of Physics, University of Augsburg, Universitätsstrasse 1, D-86135, Augsburg Germany

It is recognised now that a variety of real-life phenomena ranging from diffusion of cold atoms to motion of humans exhibit dispersal faster than normal diffusion. Lévy walks is a model that excelled in describing such superdiffusive behaviors albeit in one dimension. Here we show that, in contrast to standard random walks, the microscopic geometry of planar superdiffusive Lévy walks is imprinted in the asymptotic distribution of the walkers. The geometry of the underlying walk can be inferred from trajectories of the walkers by calculating the analogue of the Pearson coefficient.

PACS numbers: 05.40.Fb, 02.50.Ey

Introduction. The Lévy walk (LW) model [1–3] was developed to describe spreading phenomena that were not fitting the paradigm of Brownian diffusion [4]. Still looking as a random walk, see Fig. 1, but with a very broad distribution of excursions' lengths, the corresponding processes exhibit dispersal faster than in the case of normal diffusion. Conventionally, this difference is quantified with the mean squared displacement (MSD), $\langle r^2(t) \rangle \propto t^\alpha$, and the regime with $\alpha > 1$ is called superdiffusion. Examples of such systems range from cold atoms moving in dissipative optical lattices [5] to T cells migrating in the brain tissue [6]. Most of the existing theoretical results, however, were derived for one dimensional LW processes [3]. In contrast, real life phenomena – biological motility (from bacteria [7] to humans [8] and autonomous robots [9, 10]), animal foraging [11, 12] and search [13] – happen in two dimensions. Somewhat surprisingly, generalizations of the Lévy walks to two dimensions are still virtually unexplored.

In this work we extend the concept of LWs to two dimensions. Our main finding is that the microscopic geometry of planar Lévy walks reveals itself in the shape of the asymptotic probability density functions (PDF) $P(\mathbf{r}, t)$ of finding a particle at position \mathbf{r} at time t after it was launched from the origin. This is in a sharp contrast to the standard 2D random walks, where, by virtue of the central limit theorem (CLT) [14], the asymptotic PDFs do not depend on geometry of the walks and have a universal form of the two-dimensional Gaussian distribution [15, 16].

Models. We begin with a core of the Lévy walk concept [1, 2]: A particle performs ballistic moves with constant speed, alternated by instantaneous re-orientation events, and the length of the moves is a random variable with a power-law distribution. Because of the constant speed v_0 , the length l_i and duration τ_i of the i -th move are linearly coupled, $l_i = v_0 \tau_i$. As a result, the model can be

equally well defined by the distribution of ballistic move (flight) times

$$\psi(\tau) = \frac{1}{\tau_0} \frac{\gamma}{(1 + \tau/\tau_0)^{1+\gamma}}, \quad \tau_0, \gamma > 0. \quad (1)$$

Depending on the value of γ , it can lead to a dispersal $\alpha = 1$, typical for normal diffusion ($\gamma > 2$), and very long excursions leading to the fast dispersal with $1 < \alpha \leq 2$ in the case of superdiffusion ($0 < \gamma < 2$). At each moment of time t the finite speed sets the ballistic front beyond which there are no particles. Below we consider three intuitive models of two-dimensional superdiffusive dispersals.

a) The simplest way to obtain two-dimensional Lévy walk out of the one-dimensional one is to assume that the motions along each axis, x and y , are identical and independent one-dimensional LW processes, as shown in Fig 1a. The two-dimensional PDF $P(\mathbf{r}, t)$, $\mathbf{r}(t) = \{x(t), y(t)\}$, of this *product model* is given by the product of two one-dimensional LW PDFs, $P_{\text{prod}}(\mathbf{r}, t) = P_{\text{LW}}(x, t) \cdot P_{\text{LW}}(y, t)$. On the microscopic scale, each ballistic event corresponds to the motion along either the diagonal or anti-diagonal. Every re-orientation only partially erases the memory about the last ballistic flight: while the direction of the motion along one axis could be changed, the direction along the other axis almost surely remains the same. The ballistic front has the shape of a square with borders given by $|x| = |y| = v_0 t$.

b) In the *XY-model*, a particle is allowed to move only along one of the axes at a time. A particle chooses a random flight time τ from Eq. (1) and one out of four directions. Then it moves with a constant speed v_0 along the chosen direction. After the flight time is elapsed, a new random direction and a new flight time are chosen. This process is sketched in Fig. 1b. The ballistic front is a square defined by the equation $|x| + |y| = v_0 t$.

c) The *uniform model* follows the original definition by Pearson [17]. A particle chooses a random direction,

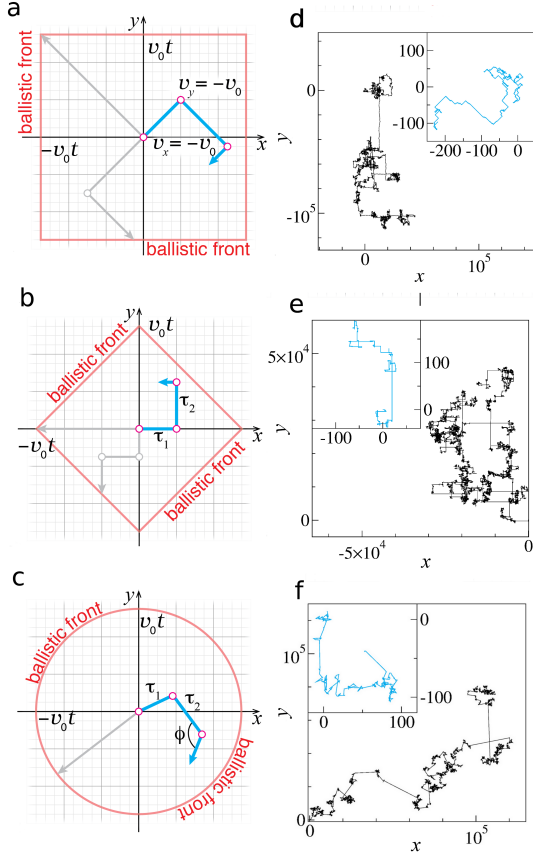


FIG. 1: **Three models of Lévy walks on a plane** a) In the *product model* x and y coordinates of a particle change according to two independent 1D Lévy walks along the coordinate axes. Whenever a direction of motion of one of the two LWs changes, there is a kink in the trajectory (\circ). The ballistic front is given by $|x| = |y| = v_0 t$ (red line). b) In *XY-model* a particle is allowed to move with a speed v_0 only along one axis at a time which is chosen randomly at the re-orientation points \circ . The ballistic front is specified by the condition $|x| + |y| = v_0 t$. c) In the *uniform model*, at each re-orientation point \circ , a particle chooses a random direction of motion, specified by an angle ϕ uniformly distributed in the interval $[0, 2\pi]$, and then moves with a constant speed v_0 . The ballistic front is a circle of the radius $v_0 t$. e-f) Trajectories produced by the models (a-b) after time $t = 10^6$. Note that on the large time scale the trajectories of the product and XY-models appear to be similar. The parameters are $\gamma = 3/2$, $v_0 = 1$ and $\tau_0 = 1$.

parametrized by the angle ϕ , uniformly distributed in the interval $[0, 2\pi]$, and then moves ballistically for a chosen flight time. The direction of the next flight is chosen randomly and independently of the direction of the elapsed flight. The corresponding trajectory is sketched in Fig. 1c. The ballistic front of the model is a circle $|\mathbf{r}| = v_0 t$.

Governing equations. We now derive equations describing the density of particles for the XY and uniform models. The following two coupled equations govern the

space-time evolution of the PDF [3]:

$$\nu(\mathbf{r}, t) = \int_0^t d\tau \int d\mathbf{v} \nu(\mathbf{r} - \mathbf{v}\tau, t - \tau) \psi(\tau) h(\mathbf{v}) + \delta(\mathbf{r}) \delta(t),$$

$$P(\mathbf{r}, t) = \int_0^t d\tau \int d\mathbf{v} \nu(\mathbf{r} - \mathbf{v}\tau, t - \tau) \Psi(\tau) h(\mathbf{v}). \quad (2)$$

The first equation describes the events of velocity reorientation [marked by \circ in Fig. 1(b-c)], where the density $\nu(\mathbf{r}, t)$ allows us to count the number of particles, $\nu(\mathbf{r}, t) d\mathbf{r} dt$, whose flights ended in the interval $[\mathbf{r}, \mathbf{r} + d\mathbf{r}]$ during the time interval $[t, t + dt]$. Velocity at each reorientation event is chosen from the model specific velocity distribution $h(\mathbf{v})$ and is statistically independent of the flight time. Second equation relates the events of velocity reorientations to the density of the particles. Here $\Psi(\tau)$ is the probability to remain in the flight for time τ , $\Psi(\tau) = 1 - \int_0^\tau \psi(t') dt'$. The formal solution of the transport equations can be found via combined Fourier-Laplace transform [18]:

$$P(\mathbf{k}, s) = \frac{\int d\mathbf{v} \Psi(s + i\mathbf{k} \cdot \mathbf{v}) h(\mathbf{v})}{1 - \int d\mathbf{v} \psi(s + i\mathbf{k} \cdot \mathbf{v}) h(\mathbf{v})} \quad (3)$$

This is a general answer for a random walk process in arbitrary dimensions with an arbitrary velocity distribution, where \mathbf{k} and s are coordinates in Fourier and Laplace space corresponding to \mathbf{r} and t respectively (but not for the product model, which is described by *two* independent random walk processes). The microscopic geometry of the process can be captured with $h(\mathbf{v})$. For the XY-model we have $h_{XY}(\mathbf{v}) = [\delta(v_y) \delta(|v_x| - v_0) + \delta(v_x) \delta(|v_y| - v_0)]/4$, while for the uniform model it is $h_{\text{uniform}}(\mathbf{v}) = \delta(|\mathbf{v}| - v_0)/2\pi v_0$. The technical difficulty is to find the inverse transform of Eq. (3). We therefore employ the asymptotic analysis [1–3] to switch from Fourier-Laplace representation to the space-time coordinates and analyze model PDFs $P(\mathbf{r}, t)$ in the limit of large \mathbf{r} and t [18].

In the diffusion limit, $\gamma > 2$, the mean squared flight length is finite. In the large time limit, the normalized covariance of the flight components in all three models is the identity matrix and so the cores of their PDFs are governed by the vector-valued CLT [25] and have the universal Gaussian shape $P(\mathbf{r}, t) \simeq \frac{1}{4\pi Dt} e^{-\frac{\mathbf{r}^2}{4Dt}}$, where $D = v_0^2 \tau_0 / [2(\gamma - 2)]$ (for the product model the velocity has to be rescaled to $v_0/\sqrt{2}$). For the outer parts of the PDFs some bounds can be obtained based on a theory developed for sums of random variables with slowly decaying regular distributions [26].

The difference between the three walks becomes sharp in the regime of sub-ballistic super-diffusion, $1 < \gamma < 2$. Figure 2 presents the PDFs of the three models obtained by sampling [18] over the corresponding stochastic processes for $t = 10^4 \gg \tau_0 = 1$. These results reveal a

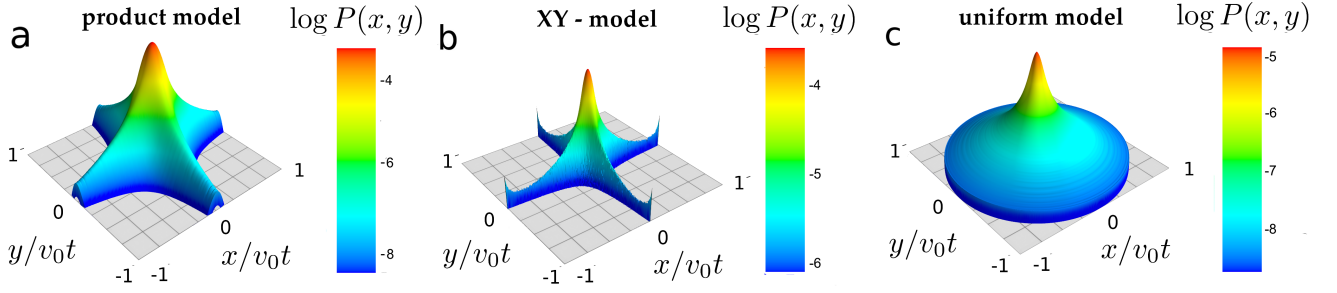


FIG. 2: **Probability density functions of the three models in the super-diffusive regime.** The distributions are plotted on a log scale for the time $t/\tau_0 = 10^4$. The PDF for the product model (a) was obtained by multiplying PDFs of two identical one-dimensional LW processes. The PDFs for the XY and uniform models were obtained by sampling over 10^{14} realizations. The parameters are $\gamma = 3/2$, $v_0 = 1$ and $\tau_0 = 1$.

striking feature, namely, that the geometry of a random walk is imprinted in its PDF. This is very visual close to the ballistic fronts, however, as we show below, the non universality is already present in the PDF cores.

The PDF of the product model is the product of the PDFs for two identical one-dimensional LWs [3]. In the case of the XY-model, the central part of the propagator can be written in Fourier-Laplace space as $P_{XY}(k_x, k_y, s) \simeq (s + \frac{K_\gamma}{2}|k_x|^\gamma + \frac{K_\gamma}{2}|k_y|^\gamma)^{-1}$, where $K_\gamma = \Gamma[2-\gamma] \cos(\pi\gamma/2) \tau_0^{\gamma-1} v_0^\gamma$ [18]. By inverting the Laplace transform, we also arrive at the product of two characteristic functions of one-dimensional Lévy distributions [27, 28]: $P_{XY}(k_x, k_y, t) \simeq e^{-tK_\gamma|k_x|^\gamma/2} e^{-tK_\gamma|k_y|^\gamma/2}$. In this case the spreading of the particles along each axis happens twice slower (note a factor 1/2 in the exponent) than in the one-dimensional case; each excursion along an axis acts as a trap for the motion along the adjacent axis thus reducing the characteristic time of the dispersal process by factor 2. As a result, the bulk PDF of the XY-model is similar to that of the product model after the velocity rescaling $\tilde{v}_0 = v_0/2^{1/\gamma}$. This explains why on the macroscopic scales the trajectory of the product model, see Fig. 1e, looks similar to that of the XY-model. The difference between the PDFs of these two models appears in the outer parts of the distributions, see Figs. 2a,b; it can not be resolved with the asymptotic analysis which addresses only the central cores of the PDFs. The PDF of the XY-model has a cross-like structure with sharp peaks at the ends, see Fig. 3a. The appearance of these Gothic-like ‘flying buttresses’ [29], capped with ‘pinnacles’, can be understood by analyzing the process near the ballistic fronts [18].

For the uniform model we obtain $P_{\text{uniform}}(\mathbf{r}, t) \simeq \frac{1}{2\pi} \int_0^\infty J_0(kr) e^{-t\tilde{K}_\gamma k^\gamma} k dk$, where $\tilde{K}_\gamma = \tau_0^{\gamma-1} v_0^\gamma \sqrt{\pi} \Gamma[2-\gamma]/\Gamma[1+\gamma/2] \Gamma[(1-\gamma)/2]$, and $J_0(x)$ is the Bessel function of the first kind (see [18] for more details). Different to the product and XY-models, this is a radially symmetric function which naturally follows from the mi-

croscopic isotropy of the walk. Mathematically, the expression above is a generalization of the Lévy distribution to two dimensions [27, 30]. However, from the physics point of view, it provides the generalization of the Einstein relation and relates the generalized diffusion constant \tilde{K}_γ to the physical parameters of the 2d process, v_0 , τ_0 and γ . In Fig. 3b we compare the simulation results for the PDF of the uniform model with the analytical expression above.

The regime of ballistic diffusion occurs when the mean flight time diverges, $0 < \gamma < 1$ [20, 21]. Long flights dominate the distribution of particles and this causes the probability concentration at the ballistic fronts. Since the latter are model specific, see Fig. 1, the difference in the microscopic schematization reveals itself in the PDFs even more clearly [18].

Pearson coefficient. The difference in the model PDFs can be quantified by looking into moments of the corresponding processes. The most common is the MSD, $\langle \mathbf{r}^2(t) \rangle = \int d\mathbf{r} \mathbf{r}^2 P(\mathbf{r}, t)$. Remarkably, for the XY- and uniform models the MSD is the same as for the 1D Lévy walk with the distribution of flight times given by Eq. (1) [18]. The MSD therefore does not differentiate between the XY- and uniform random walks (and, if the velocity v_0 is not known *a priori*, the product random walks as well). Next are the fourth order moments, including the cross-moment $\langle x^2(t)y^2(t) \rangle$. They can be evaluated analytically for all three models [18]. The ratio between the cross-moment and the product of the second moments, $PC(t) = \langle x^2(t)y^2(t) \rangle / \langle x^2(t) \rangle \langle y^2(t) \rangle$, is a scalar characteristic similar to the Pearson coefficient [31, 32]. In the asymptotic limit and in the most interesting regime of sub-ballistic super-diffusion, $1 < \gamma < 2$, this generalized Pearson coefficient equals

$$PC(t) = \begin{cases} 1, & \text{product model} \\ \frac{\gamma \Gamma[4-\gamma]^2}{\Gamma[7-2\gamma]}, & \text{XY-model} \\ \frac{(2-\gamma)^2 (3-\gamma)^2}{2(4-\gamma)(5-\gamma)(\gamma-1)} \left(\frac{t}{\tau_0}\right)^{\gamma-1} & \text{uniform model} \end{cases} \quad (4)$$

The *PC* parameter is distinctly different for the three

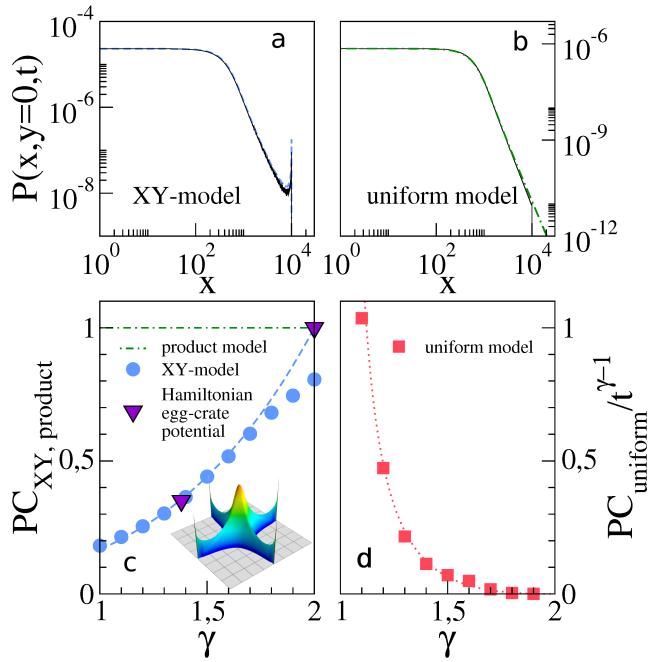


FIG. 3: **Statistical features of the models and their Pearson coefficients.** a-b) The section of the PDF of the XY model (a) and uniform model (b) along x axis. The results of the statistical sampling for $t = 10^4$ (solid black line) are compared with the analytical results (dashed lines): for the XY model it is a product of the *one-dimensional* Lévy distribution and the function $t^{1/\gamma}(t - x/v)^{-1/\gamma}$ [18], for the uniform model it is a *two-dimensional* Lévy distribution. c-d) Pearson coefficients for three models. Lines correspond to the asymptotic values Eq. (4), symbols present the results of statistical sampling for the time $t = 10^5$ (error bars are smaller than the symbol size). The PC s for the chaotic Hamiltonian diffusion in an egg-crate potential [23] at time $t = 10^5$, for energy values $E = 4$ (left triangle) and $E = 5.5$ (right triangle), was obtained by sampling over 10^5 independent realizations. The values of the exponent γ , 1.38 and 2, were extracted from the MSD exponent α , $\gamma = 3 - \alpha$. Inset shows the PDF of the process for $t = 10^3$ sampled over 10^8 realizations.

processes: the product model has the $PC(t) \equiv 1$, for the XY-model it is a constant smaller than one for any $\gamma \in]1, 2]$ and does not depend on v_0 and τ_0 , while for the uniform model it diverges in the asymptotic limit as $t^{\gamma-1}$. Figure 3 presents the $PC(t = 5 \cdot 10^5)$ of the XY- (c) and uniform models (d) obtained by samplings over 10^{14} stochastic realizations. We attribute the deviation of the numerical results for the XY-model from the analytical result Eq. (4) near $\gamma \lesssim 2$ to a slow convergence to the asymptotic limit $PC(t \rightarrow \infty)$ [18].

PC can be used to find how close is a particular two-dimensional super-diffusive process to each of the models. The value of γ can be estimated from the MSD exponent α , $\gamma = 3 - \alpha$. To test this idea we investigate a classical two-dimensional chaotic Hamiltonian system [22, 23] which exhibits a super-diffusive LW-like dynamics [4, 23]. In this system, a particle moves in a dissipationless egg-

crate potential and, depending on its total energy, exhibits normal or super-diffusive dispersals [18]. It is reported in Ref. [23] that for the energy $E = 4$ the dispersal is strongly anomalous, while in Ref. [22] it is stated that the diffusion is normal with $\alpha = 1$, within the energy range $E \in [5, 6]$. We sampled the system dynamics for two energy values, $E = 4$ and 5.5 . The obtained MSD exponents are 1.62 ± 0.04 and 1 ± 0.02 , respectively. We estimated the $PC(t)$ for the time $t = 10^5$ and obtained values 0.35 and 0.997. The analytical value of the PC (4) for the XY-process with $\gamma = 3 - 1.62 = 1.38$ is 0.355. This PC value thus suggests that we are witnessing a super-diffusive XY Lévy walk. The numerically sampled PDF of the process [18], see inset in Fig. 3c, confirms this conjecture.

In contrast to the uniform model, the PC parameters for the XY and product models are not invariant with respect to rotations of the reference frame, $\{x', y'\} = \{x \cos \phi - y \sin \phi, x \sin \phi + y \cos \phi\}$. While in theory the frame can be aligned with the directions of maximal spread exhibited by an anisotropic particle density at long times, see Fig. 2a,b, it might be not so evident in real-life settings. The angular dependence of the PC can be explored by rotating the reference frame by an angle $\phi \in [0, \pi/2]$, starting from some initial orientation, and calculating dependence $PC[\phi]$. The result can then be compared to analytical predictions for the asymptotic limit where the three models show different angular dependencies [18]. In addition, the time evolution of $PC[\phi]$ is quantitatively different for the product and XY-models and thus can be used to discriminate between the two processes. In the product model, the dependence $PC[\phi]$ changes with time qualitatively. For short times it reflects the diagonal ballistic motion of particles and for longer times attains the shape characteristic to the XY - model [18]; an effect which we could already anticipate from inspecting the trajectories in Fig. 1d. In the XY - model the positions of minima and maxima of $PC[\phi]$ are time-independent.

Conclusion. We have considered three intuitive models of planar Lévy walks. Our main finding is that the geometry of a walk appears to be imprinted into the asymptotic distributions of walking particles, both in the core of the distribution and in its tails. We also proposed a scalar characteristic which can be used to differentiate between the types of walks. Further analytical results can be obtained for arbitrary velocity distribution and dimensionality of the problem [33]. For example, it is worthwhile to explore the connections between underlying symmetries of 2D Hamiltonian potentials and the symmetries of the emerging LWs [34].

The existing body of results on two-dimensional super-diffusive phenomena demonstrates that the three models we considered have potential applications. A spreading of cold atoms in a two-dimensional dissipative optical potential [35] is a good candidate for a realization of the

product model. Lorentz billiards [36–38] reproduce the XY Lévy walk with exponent $\gamma = 2$. The uniform model is relevant to the problems of foraging, motility of microorganisms, and mobility of humans [3, 11, 12, 39, 40]. On the physical side, the uniform model is relevant to a Lévy-like super-diffusive motion of a gold nanocluster on a plane of graphite [41] and a graphene flake placed on a graphene sheet [42]. LWs were also shown, under certain conditions, to be the optimal strategy for searching random sparse targets [13, 43]. The performance of searchers using different types of 2D LWs (for example, under specific target arrangements) is a perspective topic [44]. Finally, it would be interesting to explore a non-universal behavior of systems driven by different types of multi-dimensional Lévy noise [45–47].

This work was supported by the the Russian Science Foundation grant No. 16-12-10496 (VZ and SD). IF and EB acknowledge the support by the Israel Science Foundation.

-
- [1] M. F. Shlesinger, J. Klafter, and Y. Wong, J. Stat. Phys. **27**, 499 (1982).
 - [2] M. F. Shlesinger, B. J. West, and J. Klafter, Phys. Rev. Lett. **58**, 1100 (1987).
 - [3] V. Zaburdaev, S. Denisov, J. Klafter, Rev. Mod. Phys. **87**, 483 (2015).
 - [4] J. Klafter, M.F. Shlesinger, and G. Zumofen, Phys. Today **49**, 33 (1996).
 - [5] Y. Sagi, M. Brook, I. Almog, and N. Davidson, Phys. Rev. Lett. **108**, 093002 (2012).
 - [6] T. H. Harris, E. J. Banigan, D. A. Christian, C. Konradt, E. D. Tait Wojno, K. Norose, E. H. Wilson, B. John, W. Weninger, A. D. Luster, A. J. Liu, and C. A. Hunter, Nature **486**, 545 (2012).
 - [7] C. Ariel, A. Rabani, S. Benisty, J. D. Partridge, R. M. Harshey, and A. Be'er, Nature Comm. **6**, 8396 (2015).
 - [8] D. A. Raichlen, B. M. Wood, A. D. Gordon, A. Z. P. Mabulla, F. W. Marlowe, H. Pontzer, Proc. Nat. Acad. Sci. USA **111**, 728 (2014).
 - [9] G. M. Fricke, F. Asperti-Boursin, J. Hecker, J. Cannon, and M. Moses, Adv. Artif. Life ECAL **12**, 1009 (2013).
 - [10] J. Beal, ACM Trans. Auton. Adapt. Syst. **10**, 1 (2015).
 - [11] V. Méndez, D. Campos, and F. Bartumeus, *Stochastic Foundations in Movementecology* (Springer, Berlin/Heidelberg, 2014).
 - [12] G. Viswanathan, M. da Luz, E. Raposo, and H. Stanley, *The Physics of Foraging: An Introduction to Random Searches and Biological Encounters* (Cambridge University Press, 2011).
 - [13] O. Bénichou, C. Loverdo, M. Moreau, and R. Voituriez, Rev. Mod. Phys. **83**, 81 (2011).
 - [14] B. Gnedenko and A. Kolmogorov, *Limit distributions for sums of independent random variables* (Addison-Wesley, Reading, MA, 1954).
 - [15] F. Spitzer, *Principles of Random Walks* (Springer, NY, 1976).
 - [16] J. Klafter and I.M. Sokolov, *First Steps in Random Walks* (Oxford University Press, 2011).
 - [17] K. Pearson, Nature **72**, 294 (1905).
 - [18] See Supplemental Material, which includes Refs. [19–24].
 - [19] A. Erdélyi, *Tables of Integral Transforms*, Vol. 1 (McGraw-Hill, New York, 1954).
 - [20] D. Froemberg, M. Schmiedeberg, E. Barkai, and V. Zaburdaev, Phys. Rev. E **91**, 022131 (2015).
 - [21] M. Magdziarz, and T. Zorawik, Phys. Rev. E **94**, 022130 (2016).
 - [22] T. Geisel, A. Zacherl, and G. Radons G, Phys. Rev. Lett. **59**, 2503 (1987).
 - [23] J. Klafter and G. Zumofen, Phys. Rev. E **49**, 4873 (1994).
 - [24] J. Laskar, and P. Robutel, Celest. Mech. Dyn. Astron. **80**, 39 (2001).
 - [25] A. W. Van der Vaart, *Asymptotic Statistics* (Cambridge University Press, 1998).
 - [26] A. A. Borovkov and K. A. Borovkov, *Asymptotic Analysis of Random Walks: Heavy-tailed Distributions* (Cambridge University Press, 2008).
 - [27] V. Uchaikin and V. Zolotarev, *Chance and Stability: Stable Distributions and their Applications, Modern Probability and Statistics* (De Gruyter, Berlin/New York, 1999).
 - [28] A. A. Dubkov, B. Spagnolo, and V. V. Uchaikin, Intern. J. Bifurcat. Chaos, **18**, 2649 (2008).
 - [29] J. Heyman, *The Stone Skeleton* (Cambridge University Press, 1997).
 - [30] J. P. Taylor-King, R. Klages, S. Fedotov, and R. A. Van Gorder, Phys. Rev. E **94**, 012104 (2016).
 - [31] K. Pearson, Proc. Roy. Soc. London **58**, 240 (1895).
 - [32] J. F. Kenney and E. S. Keeping, *Mathematics of Statistics*, Pt. 2 (Princeton, NJ:Van Nostrand, 1951).
 - [33] I. Fouxon, S. Denisov, V. Zaburdaev, and E. Barkai, <http://www.mpipks-dresden.mpg.de/~denysov/ubprfinal11.pdf>.
 - [34] G. M. Zaslavsky, M. Edelman, and B. A. Niyazov, Chaos **7**, 159 (1997).
 - [35] S. Marksteiner, K. Ellinger, and P. Zoller, Phys. Rev. A **53**, 3409 (1996).
 - [36] Ya. G. Sinai, Russ. Math. Surveys **25**, 137 (1970).
 - [37] J.-P. Bouchaud and A. Georges A, Phys. Rep. **195**, 127 (1990).
 - [38] G. Cristadoro, T. Gilbert, M. Lenci, D. P. Sanders, Phys. Rev. E **90**, 050102 (2014).
 - [39] N. E. Humphries, H. Weimerskirch, and D. W. Sims, Methods Ecol. Evol. **4**, 930 (2013).
 - [40] G. C. Hays, T. Bastian, T. K. Doyle, S. Fossette, A. C. Gleiss, M. B. Gravenor, V. J. Hobson, N. E. Humphries, M. K. S. Lilley, N. G. Pade, and D. W. Sims, Proc. R. Soc. B **279**, 465 (2012).
 - [41] W. D. Luedtke and U. Landamn, Phys. Rev. Lett. **82**, 3835 (1999).
 - [42] T. V. Lebedeva *et al.*, Phys. Rev. B **82**, 155460 (2010).
 - [43] G. M. Viswanathan, S. V. Buldyrev, S. Havlin, M. G. E. da Luz, E. P. Raposo, and H. E. Stanley, Nature **401**, 911 (1999).
 - [44] M. Chupeau, O. Bénichou, and R. Voituriez, Nature Phys. **11**, 844 (2015).
 - [45] A. La Cognata, D. Valenti, A. A. Dubkov, and B. Spagnolo, Phys. Rev. E **82**, 011121 (2010).
 - [46] C. Guarcello, D. Valenti, A. Carollo, B. Spagnolo, J. Stat. Mech. Theor. Exp. 054012 (2016).
 - [47] D. Valenti, C. Guarcello, B. Spagnolo, Phys. Rev. B **89**, 214510 (2014).

SUPPLEMENTAL MATERIAL

Probability density functions of 2D Lévy walks: general solution

The main mathematical tool we use to resolve the integral transport equations is the combined Fourier-Laplace transform with respect to space and time, defined as:

$$\hat{f}(\mathbf{k}, s) = \int_0^\infty dt \int d\mathbf{r} e^{-i\mathbf{k}\mathbf{r}} e^{-st} f(\mathbf{r}, t). \quad (\text{S1})$$

The coordinates in Fourier and Laplace spaces are \mathbf{k} and s respectively. The corresponding inverse transform is defined in the standard way [S1]. In the text and in the following we omit the hat sign and distinguish transformed functions by their arguments.

To find a solution to the system in Eq. (2) in the main text, we apply Fourier-Laplace transform, use its shift property,

$$\int d\mathbf{r} e^{-i\mathbf{k}\mathbf{r}} f(\mathbf{r} - \mathbf{a}) = e^{-i\mathbf{k}\mathbf{a}} \hat{f}(\mathbf{k}); \quad \int_0^\infty dt e^{-st} e^{-at} f(t) = \hat{f}(s + a). \quad (\text{S2})$$

and obtain:

$$\nu(\mathbf{k}, s) = \nu(\mathbf{k}, s) \int d\mathbf{v} \psi(s + i\mathbf{k}\mathbf{v}) h(\mathbf{v}) + 1, \quad (\text{S3})$$

$$P(\mathbf{k}, s) = \nu(\mathbf{k}, s) \int d\mathbf{v} \Psi(s + i\mathbf{k}\mathbf{v}) h(\mathbf{v}). \quad (\text{S4})$$

A system of integral equations in normal coordinates and time is reduced to a system of two linear equations for Fourier-Laplace transformed functions; it is easily resolved to give Eq. (3):

$$P(\mathbf{k}, s) = \frac{\int d\mathbf{v} \Psi(s + i\mathbf{k}\mathbf{v}) h(\mathbf{v})}{1 - \int d\mathbf{v} \psi(s + i\mathbf{k}\mathbf{v}) h(\mathbf{v})} \quad (\text{S5})$$

It is important to note that this answer is valid for both XY- and uniform models, but not for the product model.

The technical difficulty of finding the inverse Fourier-Laplace transform is the coupled nature of the problem, where space and time enter the same argument. One way to address the problem is to do asymptotic analysis. Instead of looking at full transformed functions we may consider their expansions with respect to small \mathbf{k}, s , corresponding to large space and time scales in the normal coordinates. There are two such functions in the general answer Eq. (3) in the main text, $\psi(s + i\mathbf{k}\mathbf{v})$ and $\Psi(s + i\mathbf{k}\mathbf{v})$ (note that those are Laplace transforms only, where the Fourier coordinate \mathbf{k} enters the same argument together with s). In fact their Laplace transforms are related $\Psi(s) = [1 - \psi(s)]/s$, therefore it is sufficient to show the asymptotic expansion of $\psi(s)$ for a small argument:

$$\begin{aligned} \psi(s + i\mathbf{k}\mathbf{v}) \simeq & 1 - \frac{\tau_0}{\gamma - 1} (s + i\mathbf{k}\mathbf{v}) - \tau_0^\gamma \Gamma[1 - \gamma] (s + i\mathbf{k}\mathbf{v})^\gamma \\ & + \frac{\tau_0^2}{(\gamma - 2)(\gamma - 1)} (s + i\mathbf{k}\mathbf{v})^2 + \dots \end{aligned} \quad (\text{S6})$$

Depending on the value of γ different terms have the dominating role in this expansion. Such for $\gamma > 2$ zeroth, first and second order terms are dominant, leading to the classical diffusion. In the intermediate regime $1 < \gamma < 2$ zeroth, linear and a term with a fractional power of $s + i\mathbf{k}\mathbf{v}$ are dominant and lead to the Lévy distribution.

Now by using this asymptotic expansions we can express the propagators. For example, the propagator of the uniform model in the sub-ballistic regime, after integration with respect to $h(\mathbf{v})$, has the asymptotic form:

$$P_{\text{uniform}}(\mathbf{k}, s) \simeq \frac{1}{s + |\mathbf{k}|^\gamma \frac{\tau_0^{\gamma-1} v_0^\gamma \sqrt{\pi} \Gamma[2-\gamma]}{\Gamma[1+\gamma/2] \Gamma[(1-\gamma)/2]}}. \quad (\text{S7})$$

The inverse Laplace of this expression yields an exponential function, and an additional inverse Fourier transform in polar coordinates leads to the 2D Lévy distribution discussed in the main text.

We can also write down a similar asymptotic result for the central part of the PDF in the sub-ballistic regime $1 < \gamma < 2$ for arbitrary (but symmetric) velocity distribution $h(\mathbf{v}) = h(-\mathbf{v})$, for arbitrary dimension d :

$$P(\mathbf{r}, t) \simeq \int \exp \left[i\mathbf{k} \cdot \mathbf{r} - t\tilde{A} \left| \cos \left(\frac{\pi\gamma}{2} \right) \right| \langle |\mathbf{k} \cdot \mathbf{v}|^\gamma \rangle \right] \frac{d\mathbf{k}}{(2\pi)^d}. \quad (\text{S8})$$

where $\tilde{A} = (\tau_0)^{\gamma-1} \Gamma[2-\gamma]$. The spatial statistics $P(\mathbf{r}, t)$ is controlled by the average over the velocity PDF via a function $\langle |\mathbf{k} \cdot \mathbf{v}|^\gamma \rangle$ which depends on the direction of \mathbf{k} . This is very different from the Gaussian case where only the covariance matrix of the velocities enters in the asymptotic limit of $P(\mathbf{r}, t)$. In this sense the PDF of Lévy walks Eq. (S8) is non-universal if compared with one dimensional Lévy walks, or normal d dimensional diffusion.

Difference between the XY and product models in the sub-ballistic regime

The asymptotic analysis shows that in the bulk, the XY model is identical to the product model. Therefore the cross-section of the XY PDF along the x (or y) axis is well approximated by the standard 1D Lévy distribution (see Fig. 3a,b), similarly to the product model. There is, however, a significant deviation at the tail close to the ballistic front. Let us look at the XY model closer to the front. Consider the density on the x axis, at some point $x \lesssim vt$. If a particle is that far on x axis, it means that this particle had spent at most time $t_y = t - x/v$ for its walks along the y direction. Therefore, if we look at the PDF along the y direction, it has been 'built' by only those particles which spend time t_y evolving along this direction (note that for the product model the time of walks along both directions is the same t as both walks are independent). Therefore, for a given moment of time, the PDF along x -axis of the XY model is not the 1D Lévy distribution uniformly scaled with the pre-factor $1/t^{1/\gamma}$ (as in the product model) but a product of the Lévy distribution and the non-homogeneous factor $t^{1/\gamma}/(t - x/v)^{1/\gamma}$; this pre-factor diverges as the particle gets closer to the front (see Fig. 3a) but it is integrable, so that the total number of particles is still conserved.

Probability density functions of 2D Lévy walks in the ballistic regime

For the product model, the PDF is given by the product of two PDFs of the one-dimensional Lévy walk. In the ballistic regime, PDF of the Lévy walk is the Lamperti distribution [S2]. For some particular values of γ it has a compact form. For example, for $\gamma = 1/2$ we have $P_{\text{LW}}^{(\gamma=1/2)}(x, t) = \pi^{-1}(v_0^2 t^2 - x^2)^{-1/2}$, and therefore, for 2D we get

$$P_{\text{prod}}^{(\gamma=1/2)}(x, y, t) = \frac{1}{\pi^2(v_0^2 t^2 - x^2)^{1/2}(v_0^2 t^2 - y^2)^{1/2}}. \quad (\text{S9})$$

For the XY-model, the asymptotic expression for the propagator in the ballistic regime $0 < \gamma < 1$ is

$$P_{XY}(k_x, k_y, s) = \frac{(s + ik_x v_0)^{\gamma-1} + (s - ik_x v_0)^{\gamma-1} + (s + ik_y v_0)^{\gamma-1} + (s - ik_y v_0)^{\gamma-1}}{(s + ik_x v_0)^\gamma + (s - ik_x v_0)^\gamma + (s + ik_y v_0)^\gamma + (s - ik_y v_0)^\gamma}. \quad (\text{S10})$$

For the uniform model, the answer is more compact:

$$P_{\text{uniform}}(\mathbf{k}, s) = \frac{\int_0^{2\pi} (s + ikv_0 \cos \varphi)^{\gamma-1} d\varphi}{\int_0^{2\pi} (s + ikv_0 \cos \varphi)^\gamma d\varphi}, \quad (\text{S11})$$

where $k = |\mathbf{k}|$. The integrals over the angle φ can be calculated yielding hyper-geometric functions; the remaining technical difficulty is to calculate the inverse transforms. Recently, it was shown in the one-dimensional case, that the propagators of the ballistic regime can be calculated without explicitly performing the inverse transforms [S2]. This approach has been then generalized to 2D case for the uniform model [S3], where the density of particles was shown to be described by the following expression:

$$P(\mathbf{r}, t)_{\text{uniform}} = -\frac{1}{\pi^{3/2} t^2} D_-^{1/2} \left\{ \frac{1}{x^{1/2}} \operatorname{Im} \frac{{}_2F_1((1-\gamma)/2, 1-\gamma/2; 1; \frac{1}{x})}{{}_2F_1(-\gamma/2, (1-\gamma)/2; 1; \frac{1}{x})} \right\} \left(\frac{\mathbf{r}^2}{t^2} \right) \quad (\text{S12})$$

where $D_-^{1/2}$ is the right-side Riemann-Liouville fractional derivative of order $1/2$ (see [S3] for further details). It would be interesting to try to extend this formalism to random walks without rotational symmetry, such as for example the XY model. The PDFs for the three models in the ballistic regime are shown in Fig. S1.

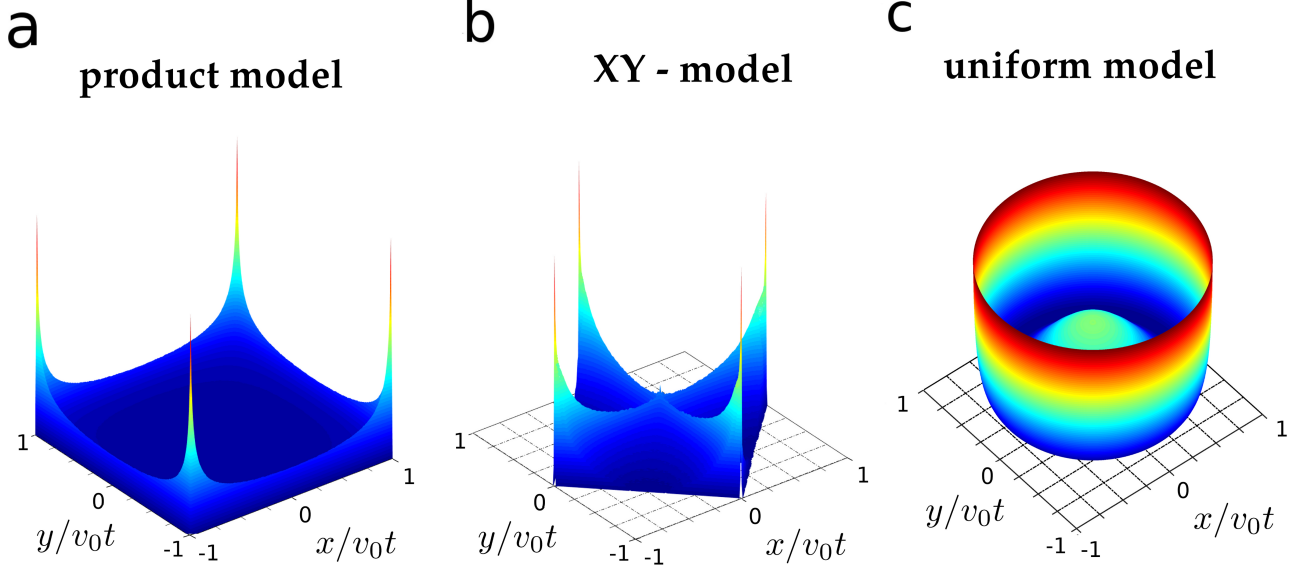


FIG. S1: Probability density functions of the three models in the ballistic regime. The PDFs for the (a) product model, (b) XY-model, and (c) uniform model are plotted on a log scale (color bars are not shown) for the time $t/\tau_0 = 10^4$. The parameters are $\gamma = 1/2$, $\tau_0 = v_0 = 1$.

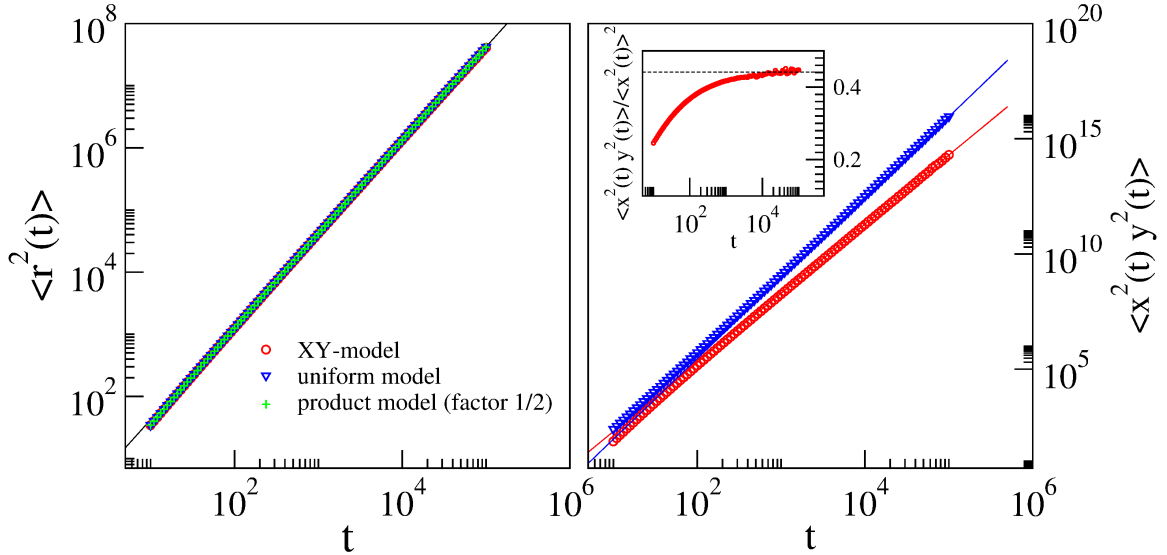


FIG. S2: Second and forth moments of the three models in the super-diffusive regime, $\gamma = 3/2$. (left panel) The MSD is identical for all three models (though the product model needs an additional prefactor of $1/2$). (right panel) The difference between the models becomes apparent in the cross-moment $\langle x^2 y^2 \rangle$. It scales as $t^{6-2\gamma}$ for the product and XY-model and as $t^{5-\gamma}$ for the uniform model. The inset shows that the convergence of the ratio between the moments to the analytical PC value (see Table S1) in course of time (number of realizations is 10^5 at every time point). The parameters are $\tau_0 = v_0 = 1$.

MSD and higher moments

In case of an unbiased random walk that starts at zero, the MSD is defined as

$$\langle \mathbf{r}^2(t) \rangle = \int d\mathbf{r} \, \mathbf{r}^2 P(\mathbf{r}, t), \quad (\text{S13})$$

Moment	$\langle r^2 \rangle$	$\langle x^4 \rangle = \langle y^4 \rangle$	$\langle x^2 y^2 \rangle$	PC
Product	$\frac{4v_0^2 \tau_0^{\gamma-1} (\gamma-1)}{(2-\gamma)(3-\gamma)} t^{3-\gamma}$	$\frac{4v_0^4 \tau_0^{\gamma-1} (\gamma-1)}{(4-\gamma)(5-\gamma)} t^{5-\gamma}$	$\frac{4v_0^4 \tau_0^{2\gamma-2} (\gamma-1)^2}{(2-\gamma)^2 (3-\gamma)^2} t^{6-2\gamma}$	1
XY	$\frac{2v_0^2 \tau_0^{\gamma-1} (\gamma-1)}{(2-\gamma)(3-\gamma)} t^{3-\gamma}$	$\frac{2v_0^4 \tau_0^{\gamma-1} (\gamma-1)}{(4-\gamma)(5-\gamma)} t^{5-\gamma}$	$\frac{v_0^4 \tau_0^{2\gamma-2} \gamma (\gamma-1)^4 \Gamma^2[1-\gamma]}{\Gamma[7-2\gamma]} t^{6-2\gamma}$	$\frac{\gamma \Gamma[4-\gamma]^2}{\Gamma[7-2\gamma]}$
Uniform	$\frac{2v_0^2 \tau_0^{\gamma-1} (\gamma-1)}{(2-\gamma)(3-\gamma)} t^{3-\gamma}$	$\frac{3v_0^4 \tau_0^{\gamma-1} (\gamma-1)}{2(4-\gamma)(5-\gamma)} t^{5-\gamma}$	$\frac{v_0^4 \tau_0^{\gamma-1} (\gamma-1)}{2(4-\gamma)(5-\gamma)} t^{5-\gamma}$	$\frac{(\gamma-3)^2 (\gamma-2)^2}{2(5-\gamma)(4-\gamma)(\gamma-1)} \left(\frac{t}{\tau_0}\right)^{\gamma-1}$

TABLE I: Asymptotic moments of the models.

The asymptotic behavior of the MSD can be calculated by differentiating the PDF in Fourier-Laplace space twice with respect to \mathbf{k} and afterwards setting $\mathbf{k} = 0$.

$$\langle \mathbf{r}^2(t) \rangle = -\nabla_{\mathbf{k}}^2 P(\mathbf{k}, t)|_{\mathbf{k}=0}. \quad (\text{S14})$$

In fact we can see from Eq. (S5) that $\nabla_{\mathbf{k}}$ applied to $P(\mathbf{k}, s)$ is equivalent to $-i\mathbf{v} \frac{d}{ds}$. Therefore all terms with the first order derivatives disappear due to the integration with a symmetric velocity distribution. Only the terms with second derivatives contribute to the answer:

$$-\nabla_{\mathbf{k}}^2 P(\mathbf{k}, s)|_{\mathbf{k}=0} = \int d\mathbf{v} \mathbf{v}^2 h(\mathbf{v}) \left\{ \frac{\Psi(s) \cdot \psi''(s)}{[1 - \psi(s)]^2} + \frac{\Psi''(s)}{1 - \psi(s)} \right\} \quad (\text{S15})$$

Now, to calculate the scaling of the MSD in real time for different regimes of diffusion, we need to take the corresponding expansions of $\psi(s)$ and $\Psi(s)$ for small s , Eq. (S6), and perform the inverse Laplace transform. As a result we obtain

$$\langle \mathbf{r}^2(t) \rangle = \begin{cases} v_0^2 (1-\gamma) t^2 & 0 < \gamma < 1 \\ \frac{2v_0^2 \tau_0^{\gamma-1} (\gamma-1)}{(3-\gamma)(2-\gamma)} t^{3-\gamma} & 1 < \gamma < 2 \\ \frac{2v_0^2 \tau_0}{\gamma-2} t & \gamma > 2 \end{cases} \quad (\text{S16})$$

It is remarkable that for $0 < \gamma < 1$ the scaling exponent of the MSD is independent of the tail exponent γ of the flight time distribution. An important observation is that the models are indistinguishable on the basis of their MSD behavior, see Fig S2 (left panel). Similarly, we compute the forth moment and find that they scale similarly for all three models (though the prefactors are model-specific, see second column in Table S1). The difference between the models become tangible in the cross-moments $\langle x^2 y^2 \rangle$. We use these moments to define a generalized Pearson coefficient which is denoted by PC ,

$$PC(t) = \frac{\langle x^2(t) y^2(t) \rangle}{\langle x^2(t) \rangle \langle y^2(t) \rangle}. \quad (\text{S17})$$

We concentrate on the sub-ballistic super-diffusive regime and summarize the corresponding results in Table S1.

Angular dependence of the Pearson coefficient

As mentioned in the main text, the value of PC depends on the choice of the coordinate frame. To quantify the dependence of the PC on the orientation of the frame of references we consider random walks $\{x'(t), y'(t)\}$ which are obtained by turning three original random walks (uniform, product and XY) by an arbitrary angle $0 \leq \phi \leq \pi/2$ with respect to the x -axis and calculate the corresponding $PC[\phi]$. The coordinates in the turned and original frames are related via:

$$\{x'(t), y'(t)\} = \{x(t) \cos \phi - y(t) \sin \phi, x(t) \sin \phi + y(t) \cos \phi\} \quad (\text{S18})$$

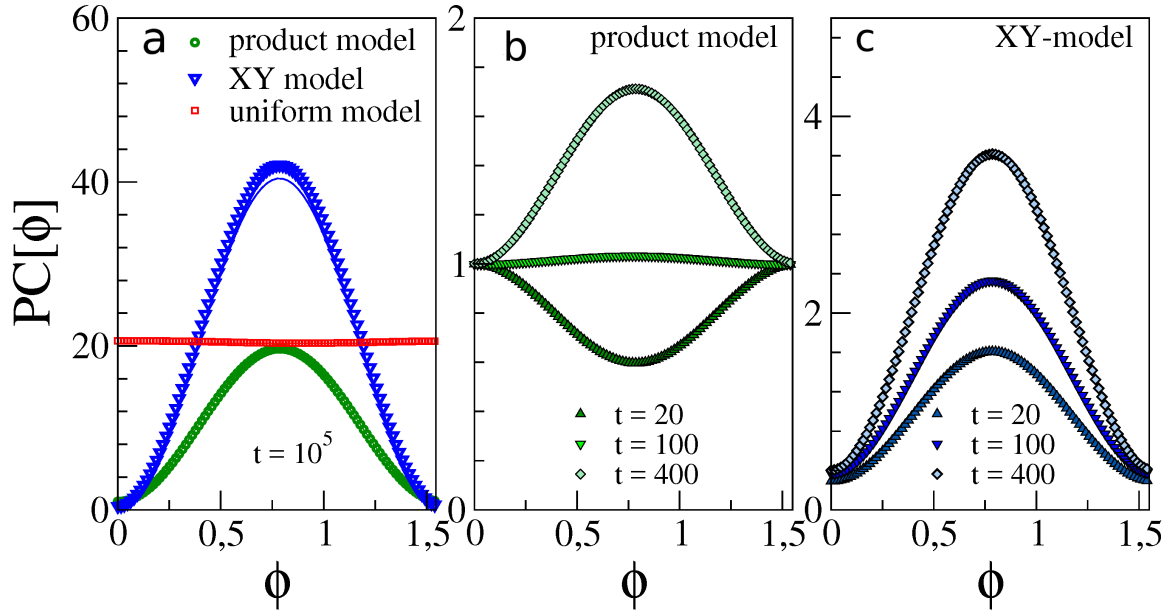


FIG. S3: Frame dependence and time evolution of the Pearson coefficient. a) Dependence of the Pearson coefficient on the frame orientation angle ϕ for the three models in the long-time limit. Symbols correspond to the results of the statistical sampling for $t = 10^5$ and lines present analytical results for the asymptotic limit, Eq. S19. b-c) Time dependence of $PC[\phi]$ for the product and XY models. For the short times, $t \lesssim 10^2$, minima of the Pearson coefficient for the product model correspond to the diagonal and anti-diagonal directions while for larger times, $t > 10^2$, these directions correspond to the maxima; minima are attained along the $\{x, y\}$ axes, see Fig. 1d in the main text. For the XY model the positions of maxima and minima are time-independent. The parameters are the same as in Fig. 2 in the main text. Note that the mean time of ballistic flights is $\langle \tau \rangle = 2$ for the chosen set of parameters.

After simple algebra and by discarding terms with odd powers of x and y , which will disappear after averaging due to symmetry, we obtain:

$$PC[\phi] = \frac{\langle x^2 y^2 \rangle (\cos^4 \phi + \sin^4 \phi - \sin^2 2\phi) + (\langle x^4 \rangle + \langle y^4 \rangle) \cos^2 \phi \sin^2 \phi}{\langle x^2 y^2 \rangle (\cos^4 \phi + \sin^4 \phi) + (\langle x^2 \rangle^2 + \langle y^2 \rangle^2) \cos^2 \phi \sin^2 \phi}. \quad (\text{S19})$$

This expression can now be evaluated by using the fourth and second-order cross moments of the original random walks given in Table S1. It can be shown that for the product and XY models and for any $\phi \neq \{0, \pi/2\}$, $PC(t; \phi) \propto t^{\gamma-1}$, whereas for the uniform model $PC(t; \phi) \propto t^{\gamma-1}$ is naturally independent of the angle ϕ . The angle dependent Pearson coefficients are different for all three models, see Fig. S3a. Importantly, the Pearson coefficient contains only one “unknown” parameter τ_0 , the scaling parameter of the flight time PDF (recall that the exponent γ of the power law tail in the flight time distribution can be determined from the scaling of the MSD). Thus by measuring the $PC(t; \phi)$, for example, at two different time points would allow for an unambiguous determination of τ_0 and of the type of the random walk model.

An interesting observation can be made by numerically calculating $PC[\phi]$ as a function of time. While the shape of the dependence remains the same for the uniform- (flat at any time) and XY-model (see Fig.S3c), for the product model it changes qualitatively. The minima of the $PC_{\text{prod}}(t; \phi)$ for short times transform into the maxima for large times passing through an intermediate flat shape, see Fig. S3b. This is a quantification of the transition we also observe by sampling individual trajectories. It is a consequence of the fact that for short times the preferred direction of motion are diagonals and anti-diagonals (inset in Fig.1d), whereas for large times the trajectories resemble those of the XY-model (Fig. 1d,e). Correspondingly the maximum of the $PC[\phi]$ “shifts” by $\pi/4$ as time progresses. At the same time, the positions of maxima and minima of $PC[\phi]$ for the XY model are time-invariant. This effect can be used to distinguish between the two models.

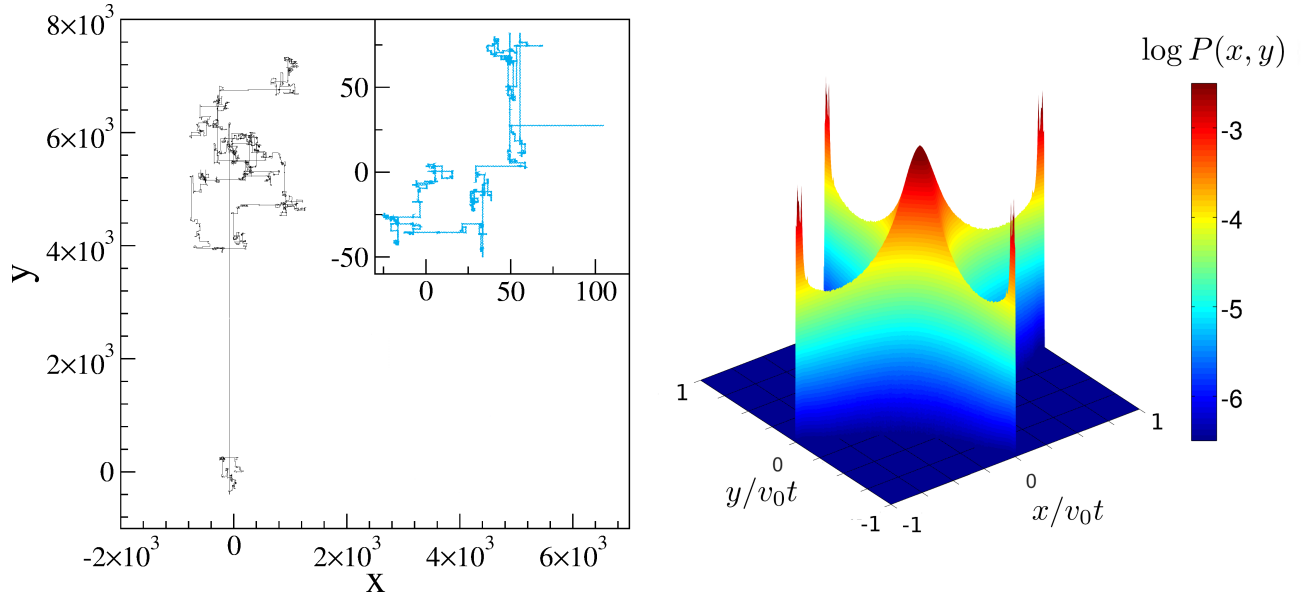


FIG. S4: Hamiltonian particle diffusion in the egg-crate potential, Eq. (S25). (left panel) A typical trajectory for $E = 4$ produced by the particle after time $t = 10^5$. Inset shows a trajectory for time $t = 10^3$; (right panel) The PDF of the corresponding dispersal process for $t = 10^3$ sampled with 10^8 realizations.

Numerical sampling procedure

The statistical sampling of the model PDFs was performed on the GPU clusters of the Max Planck Institute for the Physics of Complex Systems (Dresden) (six NVIDIA M2050 cards) and the university of Augsburg (four TESLAK20XM cards). Together with the straightforward parallelization of the sampling process this allowed us to collect up to 10^{14} realizations for every set of parameters.

Hamiltonian diffusion in an egg-crate potential

We use model from Refs. [S4,S5]. The model Hamiltonian has the form

$$H(x, y, p_x, p_y) = E = \frac{p_x^2}{2} + \frac{p_y^2}{2} + A \quad (\text{S20})$$

$$+ B(\cos x + \cos y) + C \cos x \cos y, \quad (\text{S21})$$

with particular value of the parameters $A = 2.5$ (this parameter can be dropped since it does not enter the corresponding equations of motion; however, we preserve the original form of the Hamiltonian given in Refs. [S4,S5]), $B = 1.5$, and $C = 0.5$. To integrate the equations of motion, we use the high-order symplectic integrator $SBAB_5$ [S6] with time step $\Delta t = 10^{-3}$. The energy of the system was conserved as $|\Delta E/E| < 10^{-10}$ during the whole integration time.

A typical trajectory of the system is shown on Fig. S4 (left panel). The PDF of the corresponding dispersal for time $t = 10^3$ was sampled with 10^8 realizations; the obtained result is shown in Fig. S4 (right panel). Figure S5 presents the results of numerical simulations performed to estimate Pearson coefficient PC of the dispersals for two different values of energy E .

References

- [S1] A. Erdélyi, Tables of Integral Transforms, Vol. 1 (McGraw-Hill, New York, 1954)
- [S2] D. Froemberg, M. Schmiedeberg, E. Barkai, and V. Zaburdaev, Asymptotic densities of ballistic Lévy walks. Phys. Rev. E **91**, 022131 (2015).
- [S3] M. Magdziarz, and T. Zorawik, Explicit densities of multidimensional ballistic Lévy walks, Phys. Rev. E **94**, 022130 (2016).

- [S4] T. Geisel, A. Zacherl, and G. Radons, Generic $1/f$ noise in chaotic Hamiltonian dynamics. Phys. Rev. Lett. **59**, 2503–2506 (1987).
- [S5] J. Klafter and G. Zumofen, Lévy statistics in a Hamiltonian system. Phys. Rev. **E** 49, 4873–4877 (1994).
- [S6] J. Laskar, and P. Robutel, High order symplectic integrators for perturbed Hamiltonian systems. Celest. Mech. Dyn. Astron. **80**, 39 (2001).

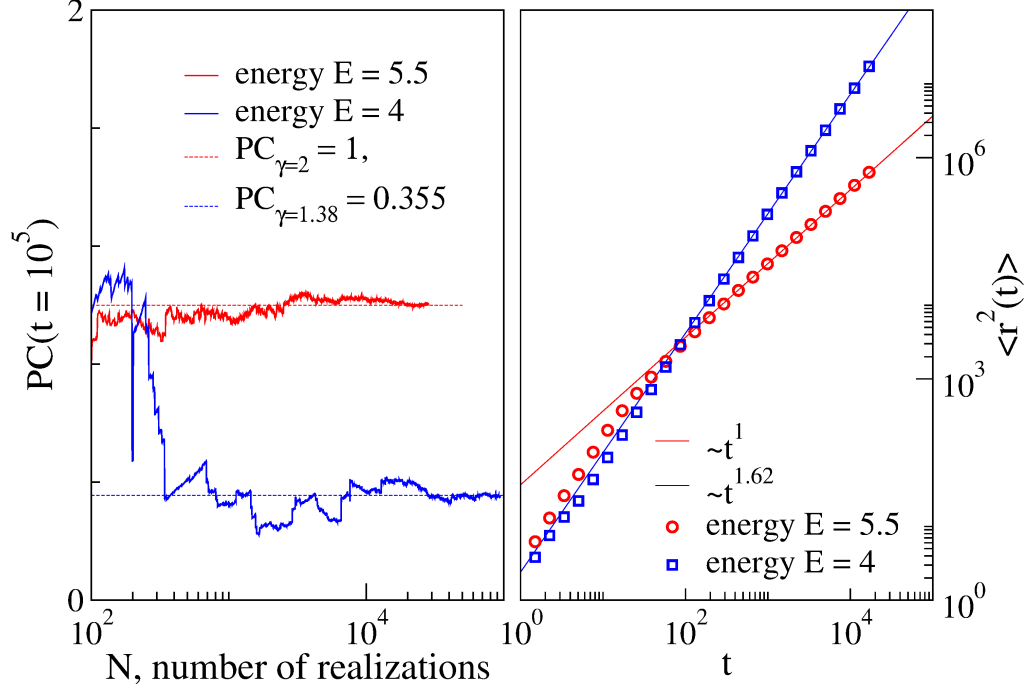


FIG. S5: Pearson coefficient and moment scaling for the Hamiltonian dispersal. PC s of the dispersals for two energy values were sampled (left panel). Plot shows Pearson coefficients for the fixed time $t = 10^5$ as a function of number of collected realizations. Thin dashed lines correspond to the analytical results, Table S1, obtained for exponents γ extracted from the MSD of the dispersals (right panel).